NUMERICAL SIMULATION OF WAVES IN FLUID SATURATED POROUS MEDIA

Juan E. Santos
Comisión Nacional de Energía Atómica
General Paz y Constituyentes - Buenos Aires
y
Consejo Nacional de Investigaciones Científicas
y Técnicas - CONICET

ABSTRACT

Biot's theory describing the propagation of waves in fluid–saturated porous solids is applied to show numerically the presence of type II compressional waves in such media, a diffusion–type wave due to the motion in opposite phase of the solid and fluid phases. The equations of motion are solved using finite element techniques and numerical results are shown and analyzed.

§ 1. INTRODUCTION

In this work we will show the application of Biot's theory [2], [3], [4], describing the propagation of waves in a fluid–saturated porous solid (which will be referred to as a Biot medium) to problems arising in exploration geophysics.

In an elastic solid, only two different types of body waves can propagate, a compressional and a shear wave. On the contrary in a Biot medium there exist two compressional waves in addition to the shear waves. In the fastest compressional wave, denoted as Type I wave, the solid and fluid constituents move in phase, while in the slower Type II wave the solid and fluid move in opposing phase. The type II waves are diffusion–type waves, suffering high attenuation over a wide range of frequencies. To observe them it is necessary to consider very high frequencies, of the order of 1 mHz. The experimental observation of this wave was first done by Plona [8], [9].

In this paper we will apply Biot's theory to describe the simulation of waves in a cilindrically symmetric domain consisting in a fluid–filled cilinder Ω_f about the centerline and z–axis $\mathcal{L}$ surrounded by a Biot medium Ω_p. After compressional point sources are exited at points in $\mathcal{L}$, the displacements are recorded at various points inside Ω_p. The organization of this paper is as follows. In Section 2 a brief review of Biot's theory is given. Then in Section 3 the model and finite element technique is described. Finally, some numerical results are shown in Section 4.

§ 2. REVIEW OF BIOT'S THEORY

Let Q denote a cube of bulk material and let $u^s = (u_i^s)$, $\widetilde{w}^f = (\widetilde{w}_i^f)$ be the averaged solid and fluid displacement vectors over Q. The fluid displacement vector is defined such that $\int_S \phi \widetilde{w}^f \cdot \nu \, d\sigma$ represents the amount of fluid displaced through the face S of Q, ϕ being the effective porosity. Let

$$w^f = \phi(\widetilde{w}^f - u^s)$$

be the fluid displacement relative to the solid frame and set

$$e = \nabla \cdot u^s , \qquad \xi = -\nabla \cdot w^f .$$

Let $\tau_{ij}(u^f, u^s)$ and $p(u^f, u^s)$ denote the total stress tensor of the bulk material and the fluid pressure. Following [4], in the isotropic case the stress–strain relations are given by

$$\begin{aligned} \tau_{ij} &= 2N\,e_{ij} + \delta_{ij}(Ae - B\xi)\,, \\ p &= -Be + M\xi\,, \end{aligned} \tag{2.1}$$

where $e_{ij} = \frac{1}{2}\left(\frac{\partial u_i^s}{\partial x_j} + \frac{\partial u_j^s}{\partial x_i}\right)$ is the solid strain tensor. Also, N is the shear modulus of the solid matrix and $A = K_c - \frac{2}{3}N$, where K_c is the bulk modulus of the saturated rock. The coefficients K_c, B and M can be computed using Gassmann theory [6] and the compressibility tests described in [5]. For completeness we include the formulas below:

$$K_c = K_s\frac{K_m + Q}{K_s + Q}\,, \quad Q = \frac{K_f(K_s - K_m)}{\phi(K_s - K_f)}\,,$$

$$B = \frac{K_s K_f(K_s - K_m)}{K_f(K_s - K_m) + K_s\phi(K_s - K_f)}\,,$$

$$M = \frac{K_s^2 K_f}{K_f(K_s - K_m) + K_s\phi(K_s - K_f)}\,.$$

Here K_s, K_m and K_f denote the bulk modulus of the solid grains, the solid matrix and the fluid, respectively.

Biot's equations of motion in the low-frequency range are

$$\begin{aligned} &\text{i)} \quad \rho\frac{\partial^2 u^s}{\partial t^2} + \rho_f\frac{\partial^2 u^f}{\partial t^2} = \nabla\cdot\tau \\ &\text{ii)} \quad \rho_f\frac{\partial^2 u^s}{\partial t^2} + g\frac{\partial^2 u^f}{\partial t^2} + b\frac{\partial u^f}{\partial t} = -\nabla p\,, \end{aligned} \tag{2.2}$$

with $\rho = (1-\phi)\rho_s + \phi\rho_f$, ρ_s and ρ_f being the solid and fluid mass densities, respectively. Also, $b = \mu/k$, where μ is the fluid viscosity, k the rock permeability and $g = S\frac{\rho_f}{\phi}$ where S is the so-called structure factor. Following [1], to estimate S we used the formula

$$S = 1 - \frac{1}{2}\left(1 - \frac{1}{\phi}\right). \tag{2.3}$$

In the high-frequency range, Biot showed that the mass and viscous coupling coefficients g and b need to be modified and become frequency dependent. Denoting by $\omega = 2\pi f$ the angular frequency, the mentioned coefficients are given by [3]

$$\begin{aligned} &\text{i)} \quad g(\omega) = \frac{\rho_f}{\phi}\left(S + \frac{F_i(\theta)}{\omega}\,\frac{\mu}{k}\,\frac{\phi}{\rho_f}\right), \\ &\text{ii)} \quad b(\omega) = \frac{\mu}{k}F_r(\theta) \end{aligned} \tag{2.4}$$

where

$$\begin{aligned} F(\theta) &= F_r(\theta) + iF_i(\theta) = \frac{1}{4}\,\frac{\theta T(\theta)}{1 + \frac{2i}{\theta}T(\theta)}\,, \\ T(\theta) &= \frac{\mathrm{ber}'\theta + i\,\mathrm{bei}'\theta}{\mathrm{ber}\,\theta + i\,\mathrm{bei}\,\theta}\,, \\ \theta &= a_p\left(\frac{\omega\rho_f}{\mu}\right)^{1/2} \end{aligned} \tag{2.5}$$

In the formulas above $ber\, z$ and $bei\, z$ are the real and imaginary parts of the Kelvin functions of the first kind and zero order. The pore-size parameter a_p in (2.5) has to be estimated from the data of the given formation. Using the form of the coefficients g and b in (2.4) implies solving the equations of motion (2.2) in the Fourier transform domain for each angular frequency ω and then obtaining the solution in the time domain by computing the inverse Fourier transform (for example using an FFT algorithm). Since results on the existence and uniqueness of the solution of (2.2) in the Fourier transform domain with the corresponding boundary conditions are still unknown, we will use in our model the low-frequency version of Biot equations, for which results on the existence and uniqueness on the solution of the equations are shown in [11].

§ 3. THE MODEL

A vertical cross-section of the domain $\Omega = \Omega_f \cup \Omega_p$ for any $\theta = \theta_0$ is shown in Figure 1 below.

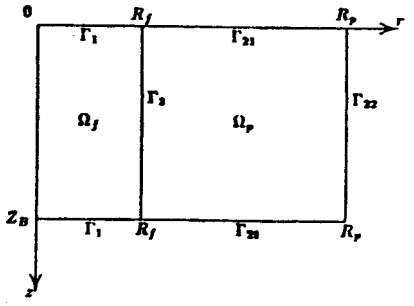

Figure 1

Let $u_1 = (u_{1r}, 0, u_{1z})$, $u_2 = (u_{2r}, 0, u_{2z})$ and $u_3 = (u_{3r}, 0, u_{3z})$ be the fluid displacement in Ω_f and the solid and fluid displacements in Ω_p. Assume zero initial displacements and velocities in both Ω_f and Ω_p and let $f_1 = f_1(r,z,t)$ be the source term in Ω_f. Then the problem is to find $u(r,z,t) = (u_1, u_2, u_3)$, $t = J = (0,T)$ such that

$$\text{i)}\quad \rho_f \frac{\partial^2 u_1}{\partial t^2} - \nabla(K_f \nabla \cdot u_1) = f_1\,, \quad (r,z,t) \in \Omega_f \times J\,,$$

$$\text{ii)}\quad \mathcal{A}\frac{\partial^2 (u_2, u_3)}{\partial t^2} + C\frac{\partial (u_2, u_3)}{\partial t} - (\nabla \cdot \tau, -\nabla p) = 0\,, \quad (r,z,t) \in \Omega_p \times J\,, \tag{3.1}$$

with boundary conditions

$$\text{i)}\ -K_f \nabla \cdot u_1 = \sqrt{\rho_f K_f}\,\frac{\partial u_1}{\partial t} \cdot \nu_f \quad (r,z,t) \in \Gamma_1 \times J\,,$$

$$\text{ii)}\ (-\tau\nu_p\nu_p, -\tau\nu_p\chi_p^1, -\tau\nu_p\chi_p^2, p) = B\Big(\frac{\partial u_2}{\partial t}\cdot\nu_p\,,\ \frac{\partial u_2}{\partial t}\cdot\chi_p^1\,,\ \frac{\partial u_2}{\partial t}\cdot\chi_p^2\,,\ \frac{\partial u_3}{\partial t}\cdot\nu_p\Big)^t\,,\ (r,z,t) \in \Gamma_2 \times J\,, \tag{3.2}$$

$$\text{iii)}\ \tau\nu_p + K_f \nabla \cdot u_1 \nu_p = 0 \quad (r,z,t) \in \Gamma_3 \times J$$

$$\text{iv)}\ (u_2 + u_3)\cdot\nu_p + u_1 \cdot \nu_f = 0 \quad (r,z,t) \in \Gamma_3 \times J$$

$$\text{v)}\ u_3 \cdot \nu_p = 0 \quad (r,z,t) \in \Gamma_3 \times J$$

In (3.2) $\nu_i = (\nu_{ir}, 0, \nu_{iz})$ $i = f,p$ is the unit outward normal on $\partial\Omega_i$ and $\chi_p{}^1$, $\chi_p{}^2$ are ortogonal unit vectors along $\partial\Omega_p$. Also the 4×4 matrices $\mathcal{A}$ and C are given by

$$\mathcal{A} = \begin{bmatrix} \rho I & \rho_f I \\ \rho_f I & gI \end{bmatrix}\,, \quad C = \frac{\mu}{k}\begin{bmatrix} 0 & 0 \\ 0 & I \end{bmatrix}\,,$$

where I is the identity matrix in $R^{2\times 2}$, $\mathcal{A}$ is positive definite and C is nonnegative.

The positive definite matrix B in (3.2) is given by [11]. Existence and uniqueness results for the system in (3.1) (3.2) were given in [11].

To formulate the finite element procedure, we proceed as follows. Let $\hat{H}(\mathrm{div},\Omega_i)$, $i = f,p$ be the closed subspace of $H(\mathrm{div},\Omega_i)$ given by

$$\hat{H}(\mathrm{div},\Omega_i) = \{\varphi = (\varphi_r,\varphi_\theta,\varphi_z) \in H(\mathrm{div},\Omega_i) : \varphi_\theta = 0\}$$

Similarly, set

$$[\hat{H}^1(\Omega_p)]^3 = \{\varphi = (\varphi_r,\varphi_\theta,\varphi_z) \in [H^1(\Omega_p)]^3 : \varphi_\theta = 0,\ \frac{\partial \varphi_r}{\partial \theta} = \frac{\partial \varphi_z}{\partial \theta} = 0\},$$

which is a closed subspace of $[H^1(\Omega_p)]^3$. Let

$$\hat{V} = \hat{H}(\mathrm{div},\Omega_f) \times [\hat{H}^1(\Omega_p)]^3 \times \hat{H}(\mathrm{div},\Omega_p)$$

and set

$$V = \{v = (v_1,v_2,v_3) \in \hat{V} : (v_2 - v_1)\cdot \nu_f = 0,\ v_3 \cdot \nu_f = 0 \quad \text{on } \Gamma_3\}$$

V is a closed subspace of the separable Hilbert space $\hat{V}$.

The weak form of problem (3.1)–(3.2) is found by multiplying equations (3.1) by test functions in V and using integration by parts. We obtain

$$\begin{aligned}
&\Big(\rho_f \frac{\partial^2 u_1}{\partial t^2}, v_1\Big)_f + \Big(\mathcal{A}\frac{\partial^2 (u_2,u_3)}{\partial t^2}, (v_2,v_3)\Big)_p + \\
&\Big(C\frac{\partial (u_2,u_3)}{\partial t}, (v_2,v_3)\Big)_p + A(u,v) + \Big\langle \sqrt{\rho_f K_f}\frac{\partial u_1}{\partial t}\cdot \nu_f, v_1\cdot\nu_f\Big\rangle_{\Gamma_1} + \\
&\Big\langle B\Big(\frac{\partial u_2}{\partial t}\cdot\nu_p, \frac{\partial u_2}{\partial t}\cdot\chi_{p^1}, \frac{\partial u_2}{\partial t}\cdot\chi_{p^2}, \frac{\partial u_3}{\partial t}\cdot\nu_p\Big)^t, \\
&(v_2\cdot\nu_p, v_2\cdot\chi_{p^1}, v_2\cdot\chi_{p^2}, v_3\cdot\nu_p)^t\Big\rangle_{\Gamma_2} \\
&= (f_1,v_1)_f, \qquad v = (v_1,v_2,v_3) \in V, \quad t \in J,
\end{aligned} \tag{3.3}$$

where $A(v,w)$ is the symmetric bilinear form defined on $\hat{V}$ by

$$\begin{aligned}
A(v,w) = {} & (K_f\nabla\cdot v_1, \nabla\cdot w_1)_f + (\tau_{rr}(v_2,v_3), \varepsilon_{rr}(w_2))_p \\
& + (\tau_{\theta\theta}(v_2,v_3), \varepsilon_{\theta\theta}(w_2))_p + (\tau_{zz}(v_2,v_3), \varepsilon_{zz}(w_2))_p \\
& + 2(\tau_{rz}(v_2,v_3), \varepsilon_{rz}(w_2))_p - (p(v_2,v_3), \nabla\cdot w_3)_p
\end{aligned} \tag{3.4}$$

The finite element procedure is defined as follows. Let $0 < h < 1$ and let τ_h^f and τ_h^p be quasiregular partitions of Ω_f and Ω_p into elements generated by the rotation of rectangles in r and z about the z–axis, with the diameter of the rectangles being bounded by h. Let $P_{1,1}(r,z)$ denote the piecewise bilinear polynomials in r and z and set

$$\mathcal{M}_h = \{\varphi = (\varphi_r,0,\varphi_z) \in C^0(\bar{\Omega}_p) : \varphi_r \in rP_{11}(r,z),\ \varphi_z \in P_{11}(r,z)\}$$

It is clear that $\mathcal{M}_h \subset [\hat{H}^1(\Omega_p)]^3$. Let $W_h(\Omega_i)$, $i = f,p$, be the vector part of the lowest order mixed finite element space defined by Morley [7]. Away from $r = 0$ the functions in $W_h(\Omega_i)$ have locally the form $\left(\frac{a}{r} + br, c + dz\right)$, while in the innermost elements about $r = 0$ have the local form $(br, c + dz)$. Then, let $\hat{V}_h = W_h(\Omega_f) \times \mathcal{M}_h \times W_h(\Omega_p)$ and set

$$V_h = \{v \in \hat{V}_h : (v_2 - v_1)\cdot \nu_f = 0,\ v_3\cdot\nu_f = 0 \quad \text{on } \Gamma_3\}$$

then $V_h \subset V$ and V_h satisfies the approximating properties [7],

$$\inf_{\varphi \in V_h} \left[\|v_1 - \varphi_1\|_{0,\Omega_f} + \|(v_2, v_3) - (\varphi_2, \varphi_3)\|_{0,\Omega_p} \right] \leq ch \left[\|v_1\|_{1,\Omega_f} + \|(v_2, v_3)\|_{1,\Omega_p} \right],$$

$$\inf_{\varphi \in V_h} \|v - \varphi\|_V \leq ch \left[\|v_1\|_{1,\Omega_f} + \|\nabla \cdot v_1\|_{1,\Omega_f} + \|v_2\|_{2,\Omega_p} + \|v_3\|_{1,\Omega_p} + \|\nabla \cdot v_3\|_{1,\Omega_p} \right].$$

In order to obtain an explicit procedure, all integrals involving time derivatives are computed using the quadrature rule

$$\int_Q f(r,z) r \, dr \, d\theta \, dz \simeq \frac{2\pi}{4} h_r h_z \sum_{i=1}^{4} f_i r_i \tag{3.5}$$

where f_i denotes the value of f at the corner a_i of the rectangle Q in the finite element partition. Let us denote by $[v,w]$ and $\langle\langle v,w \rangle\rangle$ the inner products (v,w) and (v,w) computed using (3.5).

Next, if L is a positive integer, $\Delta t = T/L$ and $U^n = U(n\Delta t)$ we set

$$d_t U^n = (U^{n+1} - U^n)/\Delta t,$$
$$\partial U^n = (U^{n+1} - U^{n-1})/(2\Delta t),$$
$$\partial^2 U^n = (U^{n+1} - 2U^n - U^{n-1})/(\Delta t)^2.$$

The discrete-time Galerkin procedure consists of finding $U^n \in V_h$, $n = 0,1,\ldots,L$ such that

$$\begin{aligned} &[\rho_f \partial^2 U_1^n, v_1]_f + [\mathcal{A}\partial^2 (U_2 U_3)^n, (v_2, v_3)]_p \\ &+ [C\partial (U_2, U_3)^n, (v_2, v_3)]_p + A(U^n, v) \\ &+ \left\langle\left\langle \sqrt{\rho_f K_f}\, \partial U_1^n \cdot \nu_f, v_1 \cdot \nu_f \right\rangle\right\rangle_{\Gamma_1} \\ &+ \left\langle\left\langle B(\partial U_2^n \cdot \nu_p, \partial U_2^n \cdot \chi_p^1, \partial U_2^n \cdot \chi_p^2, \partial U_3^n \cdot \nu_p)^t, (v_2 \cdot \nu_p, v_2 \cdot \chi_p^1, v_2 \cdot \chi_p^2, v_3 \cdot \nu_p) \right\rangle\right\rangle_{\Gamma_2} \\ &= (f_1^n, v_1)_f, \quad v \in V_h, \quad 1 \leq n \leq L-1. \end{aligned} \tag{3.6}$$

Stability and convergence results for (3.6) are given in [11]. In the next section, the procedure (3.6) will be applied to show numerically the presence of the type II compressional waves in fluid-saturated porous solids.

§ 4. A NUMERICAL EXAMPLE

The finite element procedure (3.6) was used to show numerically the presence of type II compressional waves in fluid-saturated porous rocks, as opposed to dry rocks, where only type I and shear waves can propagate. The fluid in Ω_f was taken to have density 1.4 gr/cm^3 and sound velocity 1250 m/sec. The porous material was chosen to be Teapot Sandstone with the physical data taken from [10]. The saturant fluid in Ω_p was chosen to be water of density 1 gr/cm^3 viscosity 1cp and bulk modulus 2.25×10^{10} dynes/cm^2. Setting the density, bulk modulus and viscosity of the saturant fluid in Ω_p equal to zero, and the parameter g equal to an arbitrary non zero constant, the algorithm (3.6) allows us to treat the case of dry formations. The data for the numerical tests is shown in Table 1. The compressional point sources have the form

$$f_i(r,z,t) = g(t) \nabla \delta_{r=0, z=a_i}, \; i = 1,2$$

with

$$g(t) = -2\xi(t - t_0) e^{-\xi(t-t_0)^2},$$

ξ being related to the principal frequency, chosen to be 1 mHz. The mesh size h was chosen to be .0089 cm, which is approximately 1/10 of the shortest wavelength (i.e., the type II wavelength).

The time step was chosen to be .02 μsec, which satisfies the stability constrain derived in [11]. The domain size was chosen as follows: radious of Ω_f = 2 cm, radious of Ω = 3.3 cm, Depth = 6.4 cm.

Figure 2 shows traces of the total displacement in the r–direction (i.e., $u_{2_r} + u_{3_r}$) for water saturated and dry Teapot Sandstone at the location indicated in the figure. The new event due to the arrival of the type II wave is cleary observed, with a much larger amplitude of the type II wave as compared with the type I wave.

Figure 3 shows traces of the total displacement in the r–direction for water–saturated Teapot Sandstone at a distance r = 2.1455 cm from the centerline of Ω_f and for receivers equally spaced in depth. The slopes of the lines marking the arrivals of the type I, type II and shear waves give the velocities of the corresponding waves. In a dry rock, the last event would not be present.

Figure 4 shows numerically a property of the type I and type II first shown theoretically by Biot in [2]. It can be observed that the divergence of u_2 and $\tilde{u}_2 = u_2 + \frac{1}{\phi} u_3$ have the same sign for type I waves and different signs for type II waves, showing that for the type I wave the solid and fluid move in phase while for the type II wave they move in opposite phase.

Our next objective is to include the frequency correction factors in the mass and viscous coupling coefficients g and b in Biot's equations and the effect of dissipation due to internal friction via the inclusion of frequency dependent coefficients in the stress–strain relations. This will be the subject of forthcoming publications.

REFERENCES

[1] J.G. Berryman, "Confirmation of Biot's theory", Applied Physics Letters 37 (1980), 382–384.

[2] M.A. Biot, "Theory of Propagation of Elastic Waves in a Fluid–Saturated Porous Solid. I. Low Frequency Range", J. Acoust. Soc. Amer. 28 (1956), 168–178.

[3] M.A. Biot, "Theory of Propagation of Elastic Waves in a Fluid–Saturated Porous Solid. II. Higher Frequency Range", J. Acoust. Soc. Amer. 28 (1956), 179–191.

[4] M.A. Biot, "Mechanics of Deformation and Acoustic Propagation in Porous Media", J. of Applied Physics 33 (1962), 1482–1498.

[5] M.A. Biot and D.G. Willis, "The Elastic Coefficients of the Theory of Consolidation", Journal of Applied Mechanics, Vol 24, Trans. ASME, Vol 79 (1957), 594–601.

[6] F. Gassmann, "Über die Elastizität poröser Medien", Vierteljahsschr. Naturforsch. Ges. Zürich 96 1–23 (1951).

[7] M.E. Morley, "Vector Finite Elements for Radially Symmetric Problems", to appear.

[8] T.J. Plona, "Observation of a Second Bulk Compressional Wave in a Porous Medium at Ultrasonic Frequencies", Applied Physics Letters 36 (1980), 259–261.

[9] T.J. Plona, "Acoustics of Fluid–Saturated Porous Media", in Proceedings 1982 Ultrasonics Symposium, IEEE, 1982, 1044–1048.

[10] J.H. Rosenbaum, "Synthetic Microseismograms, logging in porous formations", Geophysics 39 (1974), 14–32.

[11] J.E. Santos, J. Douglas Jr., M.E. Morley and O.M. Lovera, "Finite Element Methods for a Model for Full Waveform Acoustic Logging", IMA Journal of Numerical Analysis 8 (1988), 415–433.

Table 1
Teapot Sandstone

		Water Saturated	Dry
K	darcies	1.9	1.9
A	10^{10}dynes/cm^2	8.4044	4.3478
N	10^{10}dynes/cm^2	6.4797	6.4797
Q	10^{10}dynes/cm^2	5.3371	0
H	10^{10}dynes/cm^2	6.9197	0
ϕ		.207	.207
ρ_s	gr/cm^3	2.65	2.65
S		2.1835	2.1835

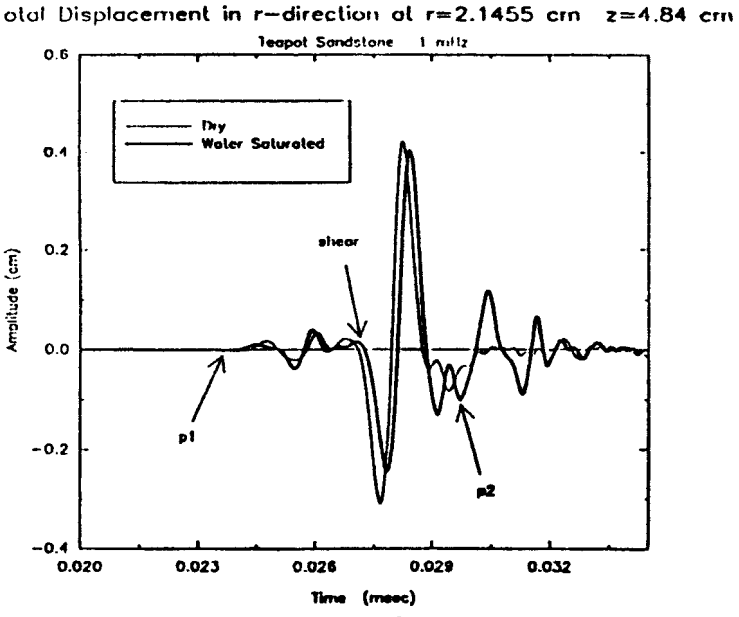

Figure 2

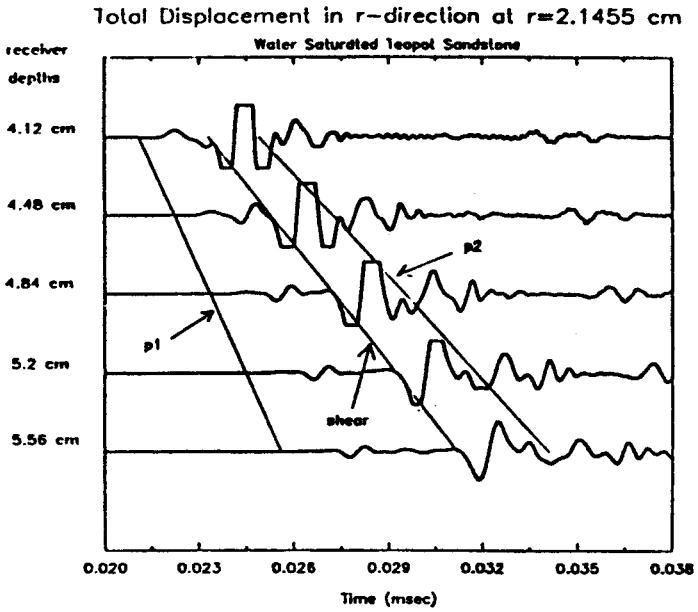

Figure 3

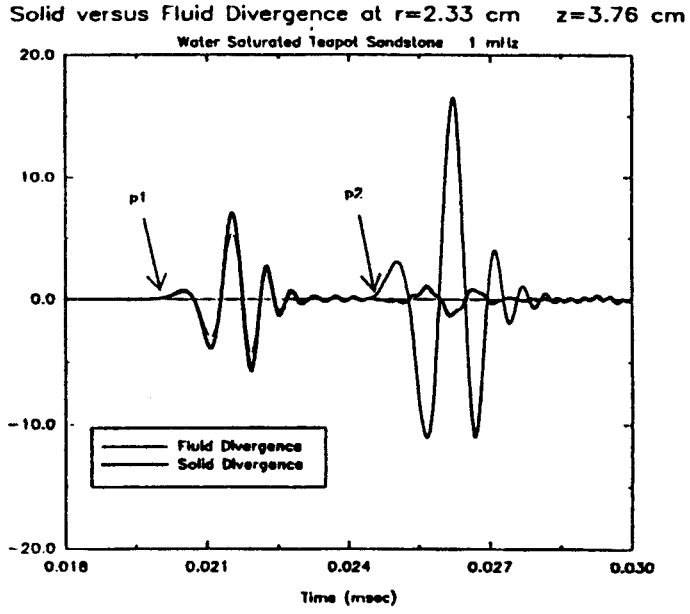

Figure 4